EUROPEAN ORGANIZATION FOR NUCLEAR RESEARCH

CERN-EP/79-42
27 April 1979

MULTIPLICITY OF CHARGED PARTICLES IN π^- INTERACTIONS ON NUCLEI AT 40 GeV/c

P.L. Frabetti
Istituto di Fisica dell'Università and INFN, Bologna, Italy

G. Bellini, M. di Corato, E. Meroni, S. Micheletti,
F. Palombo, P.G. Rancoita*), S. Sala and G. Vegni
Istituto di Fisica dell'Università and INFN, Milan, Italy

Z. Otwinowski and W. Wojcik
Experimental Physics Institute, University of Warsaw, Poland

S. Otwinowski and M. Szeptycka
Institute for Nuclear Research, Warsaw, Poland

L.P. Chernenko, Yu.I. Ivanshin, L.K. Litkin, V.A. Moiseenko,
V.I. Nikanorov, A.F. Pisarev, S.I. Sychkov, A.A. Tjapkin,
I.M. Vasilevski, V.V. Vishnjakov and O.A. Zaimidoroga
Joint Institute for Nuclear Research, Dubna, USSR

A.T. Abrosimov, G.I. Drondina, V.P. Lobanova, K.P. Vishnevskaja,
Moscow State University, Moscow, USSR

M. Pernicka
Institut für Hochenergiephysik, Österreichische Akademie
der Wissenschaften, Vienna, Austria

P. Laurikainen
High Energy Physics Department, University of Helsinki, Finland

(Submitted to Nuclear Physics B)

---

*) Present address: CERN, Geneva, Switzerland.

ABSTRACT

Multiparticle production in π^--nucleus interactions at 40 GeV/c (Fifth Joint CERN-Serpukhov Experiment) has been studied using spark-chamber technique at the Serpukhov accelerator.

The mean multiplicities, the pseudo-rapidity distributions, and the dispersion of the multiplicity distributions of charged particles produced on C, Al, Cu and Pb targets are presented.

The data have been analysed, both subtracting and including secondary protons with $p < 1$ GeV/c. In the region $\eta > 3.4$ the average multiplicity is nearly independent of the size ($\bar{\nu}$) of the target nucleus, while it increases for $\eta < 3.4$. In the forward direction ($\eta > 4$) the mean multiplicity on nuclei is smaller than the mean multiplicity on hydrogen. The dependence upon $\bar{\nu}$ in the target fragmentation region is stronger when the emitted protons are included in the pseudo-rapidity distributions of the secondary particles.

The dispersion of the multiplicity distributions for the different nuclear targets versus the mean multiplicity shows the same slope as found by the world statistics on hydrogen and by other experiments on nuclei at different energies.

The results are compared with the predictions of the coherent tube model and with the soft hadron-nucleus collision model.

1. INTRODUCTION

In recent years it has been shown that different aspects of elementary particle physics at high energies can be more easily investigated by using nuclear targets.

Further information on the hadronic production mechanism can be obtained by studying the secondary interactions inside the high-density matter of the nucleus. In this frame, strict connections exist between the space-time development of the hadron-hadron collision and detectable parameters, proper to the final state of the inclusive reactions, such as the pseudo-rapidity, the mean multiplicity, etc. [1]. The experimental data available to date pertain mostly to high energies, and up to the present time few results have been obtained below 50 GeV/c.

In this paper, data concerning pseudo-rapidity distributions and multiplicity at 40 GeV/c are presented. Data were collected on C, Al, Cu, and Pb targets at the Serpukhov accelerator.

2. EXPERIMENTAL SET-UP

The experimental set-up consisted of i) a beam-defining system, ii) the magnetic spark chamber spectrometer MIS [2], and iii) a veto beam killer.

The beam was defined by seven scintillation counters, four in coincidence and three in anticoincidence, and three Čerenkov counters, selecting π's from K's and $\bar{p}$'s (the π's represent 98% of the beam composition). The beam killer rejected non-interacting beam particles and secondary particles scattered up to an angle of 0.2° with respect to the beam direction (see fig. 1).

The MIS is a magnet with a useful volume of $1.3 \times 1.5 \times 5$ m^3, filled with 50 units of optical spark chambers with a 2 cm gap. Pictures were taken by two cameras with stereoviews at an angle of 16°.

For this experiment the targets have been placed after the first 10 spark-chamber units in order to detect the incident particles: these targets were solid

disks of C (40 and 12 mm thick), Al (20 mm), Cu (5.7 and 3.8 mm), and Pb (2.2 and 1.1 mm). Most of the pictures were taken without magnetic field in order to improve the analysis efficiency for many-prong events, and a small number were taken with a low magnetic field ($\sim$ 0.4 T).

3. PROCEDURE OF THE ANALYSIS

About 6500 pictures taken, without the magnetic field, on the C, Al, Cu, and Pb targets have been scanned. Angles of secondary tracks have been measured and the interaction vertex has been reconstructed for $\sim$ 2000 events. A weight factor has been calculated for every track, which takes into account the loss due to spark-chamber inefficiency, scanning, and measuring, and the increase due to secondary interactions inside the target, to π^0 decay, to δ-rays, and to V^0's. In addition, slow protons ($p < 1$ GeV/c) have been subtracted: their contribution has been estimated using a sample of $\sim$ 400 events taken with a low magnetic field. Slow tracks ($p < 1$ GeV/c) were reconstructed in space and their momenta were measured. The number of slow protons was obtained as the difference between the number of positive and negative tracks assuming that π^+ and π^- with $p < 1$ GeV/c are produced with the same frequency.

3.1 Inefficiency in detecting and measuring tracks

Only the tracks crossing at least six spark chamber units have been taken into account in order to have a high detection efficiency. This corresponds to defining an acceptance cone of $\pm 40^\circ$ with respect to the beam. Inside this cone the detection inefficiency is less than 0.5% on the average. Accurate corrections have been calculated after scanning a sample of tracks, spark by spark, as a function of the topology of the events and of the angle of the track with respect to the chamber plates and to the distance from the vertex of the event.

The pictures were scanned twice. For a few events the track matching was unsuccessful for some prongs. This happened for $\sim$ 1% of the tracks, and corrections were introduced to take into account this effect.

Two tracks with an opening angle < 7 mrad can be interpreted as one track owing to the limited resolution of spark chambers. This effect is not negligible in the very forward direction, where a correction lower than 1% had to be introduced.

The interaction vertex is reconstructed using the secondary tracks and that of the beam. Tracks not pointing to the vertex within 4 standard deviations were rejected. The rejected tracks correspond to $\sim$ 1% of the total number of prongs.

3.2 Secondary interactions

The total sample of prongs contains particles produced in secondary interactions inside the target. Their contribution was estimated by a Monte Carlo calculation. In this calculation total inelastic cross-sections for the π^--nucleus at different energies, deduced from the compilation of Barashenkov and Toneev [3] have been used.

The mean value of the multiplicity and the pseudo-rapidity distribution for charged particles produced in secondary hadron-nucleus interactions were assumed to depend only on the effective energy of the reaction. The effective energy was calculated taking the target nucleus as being equivalent to the mean number of nucleons seen by the incident particle traversing the nucleus (see Gottfried [4]).

The mean multiplicity is assumed to be a phenomenological function of the effective energy [5]. The multiplicity distribution is calculated using KNO scaling starting from bubble-chamber π^--C data at 40 GeV/c [5,6]. The pseudo-rapidity distributions were obtained from the π^--C data scaling the mean value in the variable $\eta/\ln s$ *). The momenta were generated assuming a p_T^2 distribution, independent of the incident energy.

3.3 π^0 decay

The e^+e^- tracks coming from π^0 decay and materialization of the γ's inside the target have been subtracted by a Monte Carlo calculation. Wroblewski [7] shows how $\langle n_{\pi^0} \rangle$ (the average number of π^0's produced on the proton at fixed charged

*) The pseudo-rapidity η is defined as $-\ln[\mathrm{tg}(\theta_{lab}/2)]$.

topology) changes with $\langle n_{ch} \rangle$ (the average number of charged particles). A similar behaviour is also assumed for the interactions on nuclei, when the average multiplicity is the same as the multiplicity on the proton. It is thus possible to obtain $\langle n_{\pi^0} \rangle$ versus $\langle n_{ch} \rangle$ [6,8,9] for 40 GeV/c π^- interacting on C, Al, Cu, and Pb. The rapidity distribution of π^0 is assumed to be the same as the distribution of charged particles.

The e^+e^- tracks from γ's materializing in the targets are subtracted from the charged prongs when their projected aperture angle is larger than 7 mrad; otherwise one track is subtracted.

3.4 V^0 production and δ-rays

The production of V^0 particles in π^--p and π^--C interactions at 40 GeV/c has been studied in a propane bubble chamber [6,8]. Extrapolating the results obtained on proton and carbon to Al, Cu, and Pb, it is possible to estimate the correction to be applied to our data for the V^0's decaying inside the target.

With regard to the δ electrons, the probability of mistaking a δ track for a charged secondary has been calculated with the standard formulae.

3.5 Corrections

The corrections applied to every track, which take into account the effects described above, are summarized in table 1. The larger correction comes from the π^0 decay (fourth column) and shows an upper limit of $\sim$ 10% for the Cu target.

4. RESULTS

The results presented in this paper concern the mean multiplicity values for different regions of pseudo-rapidity and the pseudo-rapidity distributions for the total sample of tracks and fixed ranges of multiplicity. Only events with charged multiplicity $N \geq 2$ have been considered. The events with one prong are already strongly depressed at trigger level by the veto beam killer counter, the aim being to reject most of the elastic scatterings. The coherent events were also subtracted from the experimental sample.

Events are considered as coherent processes if they fulfil one of the following requirements: either their prongs are produced inside a cone of $\pm[3.5° + (N/2)°]$, or $\sum_N \theta < 3° \cdot N$ (θ is the production angle in the lab. system). Both these criteria give the same percentage of rejection: 2.5 ± 0.3%, 0.5 ± 0.1%, 0.1 ± 0.1% for three-, five-, and seven-prong events, respectively.

As explained in Sections 2 and 3.1, the acceptance region is defined for $1 \leq \eta \leq 6.28$.

All the results are calculated with and without slow protons ($p < 1$ GeV/c). The evaporation protons ($p < 300$ MeV/c) do not really contribute to the sample of slow protons, because of the absorption in the target, except in the case of the 1.1 mm thick lead target, where their contribution is smaller than 1.5% of the number of prongs.

4.1 Multiplicity

The average multiplicity for charged secondaries has been calculated in four different regions of pseudo-rapidity: (1.0-2.0), (2.0-3.0), (3.0-4.0), (4.0-6.28), for the samples with and without slow protons. The results are presented in table 2; the errors include the statistical fluctuations and the uncertainties in the slow protons subtraction.

The ratio R_A between the average multiplicity on the nucleus and the average multiplicity on hydrogen has been calculated using data obtained in a propane bubble chamber with incident π^- of 40 GeV/c [6,8,10]. In that experiment, the events were classified as interactions on hydrogen when, as usual, the charge balance was satisfied and no more than one small recoil was visible. Because of these criteria, all the direct interactions on the bound proton without visible evaporation tracks are included in the sample on hydrogen. Also in the sample on hydrogen, as in the data on nuclei, events with $N < 2$ in the acceptance cone of ±40° are rejected.

The ratio R_A for samples without slow protons is obtained using data on hydrogen after having subtracted protons with $p < 0.7$ GeV/c. This momentum is the upper

limit of reliability for recognizing protons in a propane bubble chamber, using ionization. The diffractive dissociation events are not subtracted from the events on hydrogen.

In figs. 2 and 3, R_A versus $\bar{\nu}$ ($= A \cdot \sigma^{inel}_{\pi^- p} / \sigma^{inel}_{\pi^- A}$) is plotted. The main features of these distributions can be summarized as follows:

i) In the very forward direction ($4 < \eta < 6.28$), R_A is constant and always < 1. This is true also if we correct the data for the diffraction dissociation events, which are rejected from the samples on nuclei but not from the data on H: their contribution in any case does not exceed the quoted errors.

ii) In the η range 3-4, R_A versus $\bar{\nu}$ is consistent within 2 standard deviations with a flat behaviour.

iii) For $\eta < 3$, R_A increases with $\bar{\nu}$ as η becomes smaller.

iv) Similar behaviour is shown by the samples with and without protons with $0.3 < \beta < 0.7$.

The results on carbon agree with those obtained on the same nucleus in the propane bubble chamber experiment [10], where protons with $p < 250$ MeV/c are rejected.

4.2 Pseudo-rapidity

The pseudo-rapidity distributions for the data with and without protons are shown in figs. 4 and 5. In the vertical axis $(1/n_{ev})(\Delta N/\Delta\eta)$ is plotted versus η (where N is the number of charged tracks and n_{ev} is the total number of events). The distributions overlap in 1 standard deviation, for $\eta > 3.4$. For η between 1 and 3.4, i.e. in the central and target fragmentation regions $(1/n_{ev})(\Delta N/\Delta\eta)$ increases greatly with the atomic weight of the target. This effect is larger in the distributions with slow protons.

In fig. 6 the pseudo-rapidity distributions, normalized to the same area, are plotted for events with fixed topology, in order to understand to what extent the nucleus target affects the shape of the distributions; $(1/N)(\Delta N/\Delta\eta)$ is plotted

versus η, and the events are divided into four regions of charged multiplicity: 2-4, 5-7, 8-10, and 11-13. The full-line curves represent the pseudo-rapidity distributions, obtained on C from the propane bubble chamber experiment, in the same multiplicity regions [10].

The same behaviour as shown by the different distributions at fixed multiplicity leads us to conclude that the multiplicity, and not the nucleus target, determines the shape of the pseudo-rapidity distributions.

4.3 Dispersion of the multiplicity distributions

In fig. 7 the dispersion $D = \sqrt{\langle N^2 \rangle - \langle N \rangle^2}$ is plotted versus $\langle N \rangle$ for the samples with and without protons in the β range: 0.3-0.7. As usual in this experiment, only the region with $\eta > 1$ is taken into account. Different fits to $D = A + B \langle N \rangle$ on both the samples yields, for A and B, values quite consistent with the best fits obtained on the $\pi^- p$ world statistics ($A = 0.56 \pm 0.01$; $B = 0.58 \pm 0.07$ [7] and on π^--nucleus data in a large energy range (10-200 GeV [11]). This dispersion of the multiplicity distribution on hydrogen (bubble-chamber data [10]) for $\eta > 1$ lies on the same straight line.

5. COMPARISON WITH THEORETICAL PREDICTIONS

The pseudo-rapidity distributions obtained in this experiment have been compared with those expected from theoretical models, such as the coherent tube model (CTM) [12] and the soft hadron-nucleus collision model (SCM) [13]. The comparison of results on the average multiplicity is more difficult because of the limited angular acceptance of the experimental apparatus.

5.1 Coherent tube model

The CTM predictions have been calculated by Bergström and Fredriksson [14] who used the following procedure:

i) The produced particles have been classified as either beam fragments, central particles, or target fragments.

ii) Beam fragments and central particles are assumed to be independent of the quantum numbers of the target. The following formula has been used:

$$\left.\frac{1}{n_{ev}^{\pi A}}\frac{dN^{\pi A}}{d\eta}\right|_{\substack{\text{without}\\ \text{tube fragm.}}}(p_{beam},\eta) = \left.\frac{1}{n_{ev}^{\pi n}}\frac{dN^{\pi n}}{d\eta}\right|_{\substack{\text{without}\\ \text{n fragm.}}}(A^{1/3}\,p_{beam},\ \eta+\ln A^{1/3}) \ , \quad (1)$$

which, applied to π^- interactions at 40 GeV/c on C, Al, Cu, and Pb, needs π^-n data at 92, 120, 160, and 240 GeV/c, respectively. To get the spectra on Pb, the data of Azimov et al. [15] obtained in emulsion at 200 GeV/c can be used, with some approximation. No useful data exist for the other energies.

iii) For the tube fragments, the following simple scaling law [16] is used:

$$\left.\frac{1}{n_{ev}^{\pi A}}\frac{dN^{\pi A}}{d\eta}\right|_{\substack{\text{tube}\\ \text{fragm.}}}(p_{beam},\eta) = A^{1/3}\ \left.\frac{1}{n_{ev}^{\pi n}}\frac{dN^{\pi n}}{d\eta}\right|_{\text{n fragm.}}(p_{beam}\,A^{-1/3},\eta) \ . \quad (2)$$

The data of Crennell et al. [17] and Bosetti et al. [18] on $\pi^-p \to pX$ provide information on target fragmentation in 7 GeV/c (π^--n) interactions, which is needed to apply formula (2) to 40 GeV/c (π^--Pb) spectra.

In fig. 8 the η distributions obtained in this experiment from π^--Pb data (histograms) are compared with the predictions of the CTM (continuous curves): full lines correspond to the distributions without protons with $\beta < 0.7$; dotted lines include protons with $\beta > 0.3$. The consistency of the model expectation with the experimental data is good for the distributions without slow protons. The spectra including protons with $0.3 < \beta < 0.7$ show higher values with respect to the corresponding theoretical curves in the region $1.4 < \eta < 2.2$.

5.2 Soft collision model

The procedure used in calculating the predictions of the SCM are described elsewhere [19,20]. The comparison with the results of the present experiment has been carried out following the procedure described below:

i) The theoretical calculation produces differential multiplicities as a function of the rapidity variable, while the experimental data give the pseudo-rapidity variable. This problem has been solved using results coming from the experiments of Angelov et al. and Abdurakhimov et al. [10] and Ferbel [21], where angles and momentum of the secondary particles were measured. The pseudo-rapidity distribution compared with the rapidity spectrum calculated for the same tracks shows a shift that is nearly constant in all the η range. Consequently our histograms are shifted in the same way, simply changing the horizontal scales, as shown in fig. 9.

ii) The SCM predictions are compared with the experimental distributions without slow protons, because the SCM really neglects the slow recoils.

iii) The rapidity distribution from the elementary hadron-hadron collision is the only input of the theoretical calculation. An interpolating formula has been used for this purpose [21]. In making a comparison with the present data, it was considered that a more reliable procedure would be to normalize the theoretical curve for carbon to the same area of the corresponding experimental histogram and to calculate the curves for the other nuclei with respect to that for carbon. The curve has been normalized, taking into account only the area included in the η range (1.4-3.4), where the cut on one-prong events does not contribute.

Figure 9 shows the comparison. The over-all agreement between the shape of the calculated curves and that of the data is fairly good, but for the interactions on Pb the experimental histogram is a little lower than the curve.

6. CONCLUSIONS

The general features of the mean multiplicities and the pseudo-rapidity distributions found in this experiment are not very different from those obtained at higher energy.

Nevertheless some very important new types of behaviours are shown by the present data:

i) In the forward direction ($\eta > 4$), the multiplicity on nuclei is smaller than the multiplicity on hydrogen.

ii) The pseudo-rapidity distributions change with the multiplicity of the events and not with the nucleus target.

In addition, the slope of the dispersion of the multiplicity distributions as a function of the average multiplicity, which is independent of the incident energy and of the target, is not affected by the cuts on pseudo-rapidity.

The comparison with the CTM and the SCM gives a fairly good agreement in both cases, not allowing one to discriminate between them.

REFERENCES

[1] See for example: W. Busza, Proc. 6th Int. Conf. on High-Energy Physics and Nuclear Structure, Santa Fe and Los Alamos, 1975, AIP Conf. Proc. No. 26, ERDA Conf. 75063 (American Institute of Physics, New York, 1975); p. 211; L. Bertocchi, ibid., p. 238; and the papers cited therein.

[2] G. Bellini, Proc. Topical Meeting on Multiparticle Production on Nuclei at very High Energy, Trieste, 1976 (IAEA-SMR-21, Trieste, 1977), p. 503.

[3] W.S. Barashenkov and W.D. Toneev, Interaction of high-energy particles and nuclei with nuclei (Atomizdat, Moscow, 1972).

[4] K. Gottfried, Proc. 5th Int. Conf. on High-Energy Physics and Nuclear Structure, Uppsala, 1973 (North-Holland, Amsterdam. 1973), p. 79.

[5] O. Czyzewski and K. Rybicki, Nuclear Phys. B47 (1972) 633.

[6] N. Angelov et al., JINR preprints: P1-814 (Dubna, 1974); P1-9792, P1-9882, P1-10163, P1-10324 (Dubna, 1976).

[7] A. Wroblewski, Proc. 8th Int. Symposium on Multiparticle Dynamics, Kayserberg, 1977 (Centres de recherches nucléaires, Strasbourg, 1977), p. 37.

[8] A. Abdurakhimov et al., Nuclear Phys. 20 (1974) 384; preprint P1-8566 (Dubna, 1975).

[9] W. Busza et al., Phys. Rev. Lett. 34 (1975) 836; Proc. Topical Meeting on Multiparticle Production on Nuclei at very High Energies, Trieste, 1976 (IAEA-SMR-21, Trieste, 1977).

[10] N. Angelov et al., private communication.
A. Abdurakhimov et al., private communication.

[11] W. Busza, Acta Phys. Polon., B8, 333, 1977.

[12] See for example: S. Fredriksson *in* Proc. Triangle Seminar on Recent Developments in High-Energy Physics, Campione d'Italia, 1977 (Ed. Compositori, Bologna 1978), p. 381, and preprint CERN-TH 2423 (1977), and references given therein.
L. Bergström and S. Fredriksson, preprint CERN-TH 2505 (1978).

[13] A. Capella and A. Krzywicki, Phys. Letters, B67 (1977) 84, and Invited contribution to the Triangle Seminar on Recent Developments in High-Energy Physics, Campione d'Italia, 1977 (Ed. Compositori, Bologna 1978), p. 369.

[14] S. Fredriksson, private communication.

[15] S.A. Azimov et al., Nuclear Phys. B129 (1977) 205; and paper contributed to the 7th Int. Conf. on High-Energy Physics and Nuclear Structure, Zurich, 1977.

[16] L. Bergström and S. Fredriksson, Phys. Letters 68B (1977) 177.

[17] D.J. Crennel et al., report BNL-16417 (1971).

[18] P. Bosetti et al., Nuclear Phys. B54 (1973) 141.

[19] A. Capella and A. Krzywicki, preprint LPTPE 77/1, to be published in Phys. Rev. D.

[20] A. Krzywicki, Invited talk given at the Meeting on Hadron Physics at very High Energies, Marseille, 1978 (to be published).

[21] T. Ferbel, reference included in: C. Halliwell, Invited paper at the 8th Int. Symposium on Multiparticle Dynamics, Kayseberg, 1977 (Centres de recherches nucléaires, Strasbourg, 1977), p. 234.

Table 1

Corrections applied to every track

Target	Lost tracks	Secondary interactions	π^0 production	V^0 production	δ-rays
C	+0.019	-0.019	-0.043	-0.004	-0.013
Al	+0.016	-0.020	-0.087	-0.004	-0.013
Cu	+0.041	-0.020	-0.097	-0.004	-0.011
Pb	+0.042	-0.005	-0.077	-0.004	-0.003

Table 2a

Average multiplicity of charged secondaries including protons with $\beta > 0.3$

Target \ η	1.0-2.0	2.0-3.0	3.0-4.0	4.0-6.28
C	$1.71 \begin{smallmatrix}+0.05\\-0.07\end{smallmatrix}$	1.99 ± 0.06	1.44 ± 0.05	0.66 ± 0.06
Al	$2.00 \begin{smallmatrix}+0.06\\-0.09\end{smallmatrix}$	2.30 ± 0.06	1.67 ± 0.05	0.63 ± 0.06
Cu	$2.55 \begin{smallmatrix}+0.08\\-0.14\end{smallmatrix}$	2.49 ± 0.08	1.61 ± 0.06	0.71 ± 0.06
Pb	$3.11 \begin{smallmatrix}+0.09\\-0.16\end{smallmatrix}$	2.63 ± 0.08	1.52 ± 0.06	0.64 ± 0.06

Table 2b

Average multiplicity of charged secondaries, once subtracted protons with $\beta < 0.7$

Target \ η	1.0-2.0	2.0-3.0	3.0-4.0	4.0-6.28
C	1.57 ± 0.12	1.96 ± 0.06	1.44 ± 0.05	0.66 ± 0.06
Al	1.70 ± 0.15	2.23 ± 0.06	1.67 ± 0.05	0.63 ± 0.06
Cu	2.11 ± 0.16	$2.39^{+0.07}_{-0.08}$	1.61 ± 0.06	0.71 ± 0.06
Pb	2.41 ± 0.17	2.50 ± 0.08	1.51 ± 0.06	0.64 ± 0.06

Figure captions

Fig. 1 : Sketch of the experimental set-up.

Fig. 2 : The ratio $R = \langle n \rangle_A / \langle n \rangle_H$ is plotted as a function of $\bar{\nu}$, not including evaporation protons ($\beta > 0.3$) for different pseudo-rapidity regions.

Fig. 3 : The ratio $R = \langle n_A \rangle / \langle n \rangle_H$ is plotted as a function of $\bar{\nu}$, when all the protons with $\beta < 0.7$ are subtracted, for different pseudo-rapidity regions.

Fig. 4 : Distributions of the pseudo-rapidity for the different nuclear targets, including protons with $\beta > 0.3$, compared with bubble-chamber data at 40 GeV/c.

Fig. 5 : Distributions of the pseudo-rapidity for the different nuclear targets, when protons with $\beta < 0.7$ are subtracted, compared with bubble-chamber data at 40 GeV/c.

Fig. 6 : Pseudo-rapidity distributions for different charged multiplicity are shown versus nuclear targets. The full-line curves represent the pseudo-rapidity distributions obtained on carbon from propane bubble-chamber data, normalized to the same area.

Fig. 7 : The dispersion of the multiplicity distributions is plotted versus the mean multiplicity. The straight line corresponds to the best fit to the world $\pi^- p$ statistics [7].

Fig. 8 : Comparison of the π^--Pb data of this experiment with the predictions of the CTM. The dotted lines correspond to the data including protons with $\beta > 0.3$, the full lines to the distribution without protons with $\beta < 0.7$.

Fig. 9 : SCM predictions drawn for different A and compared with experimental distributions without protons with $\beta < 0.7$.

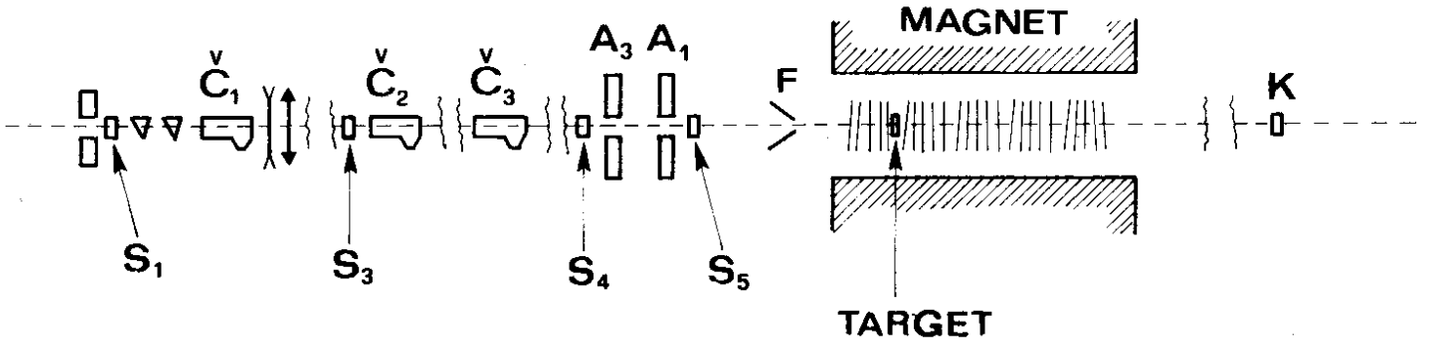

Fig. 1

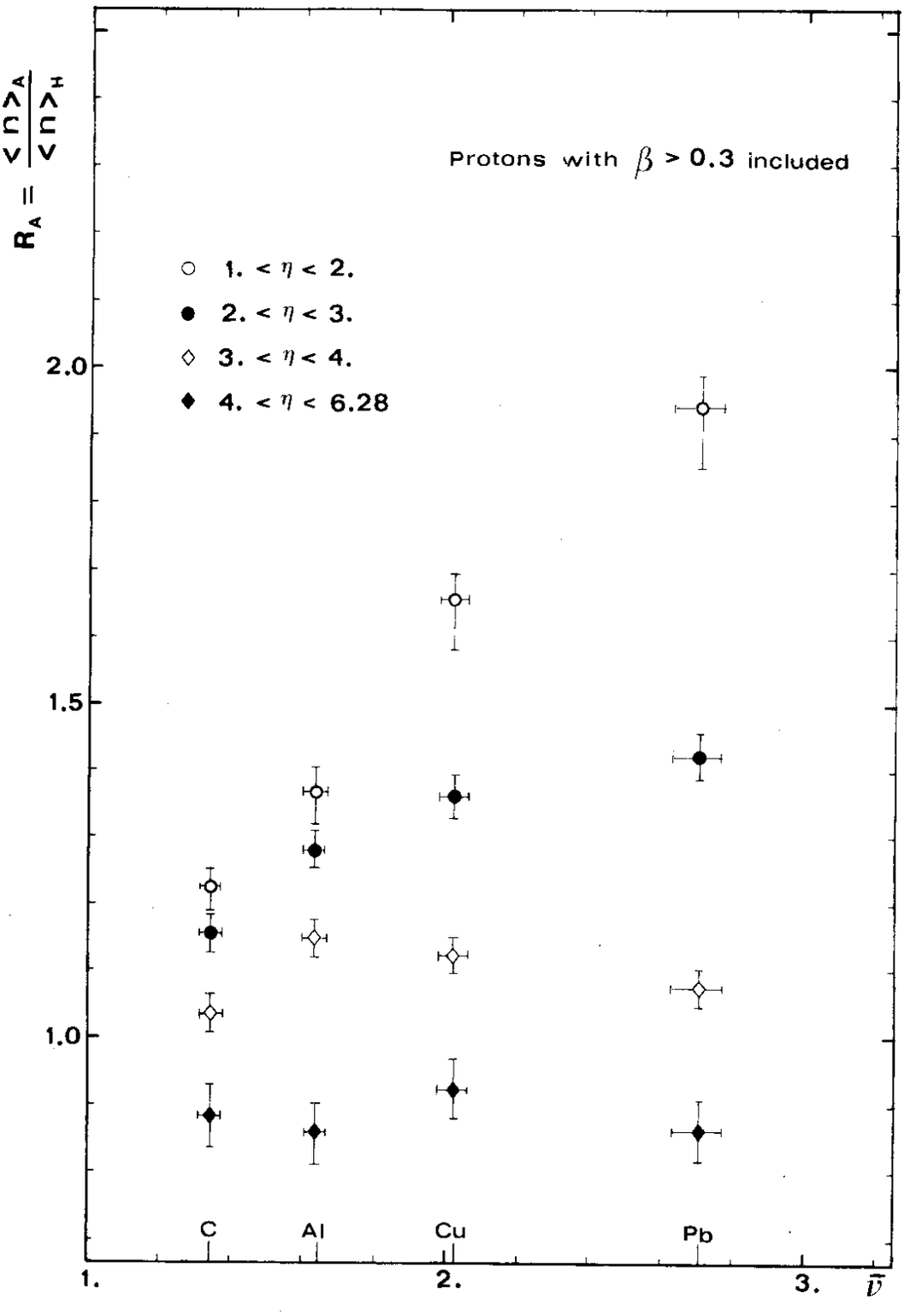
$R_A = \frac{\langle \nu \rangle_A}{\langle \nu \rangle_H}$
Protons with $\beta > 0.3$ included
○ 1. < η < 2.
● 2. < η < 3.
◇ 3. < η < 4.
◆ 4. < η < 6.28
2.0
1.5
1.0
C
Al
Cu
Pb
1.
2.
3.
$\bar{\nu}$

Fig. 2

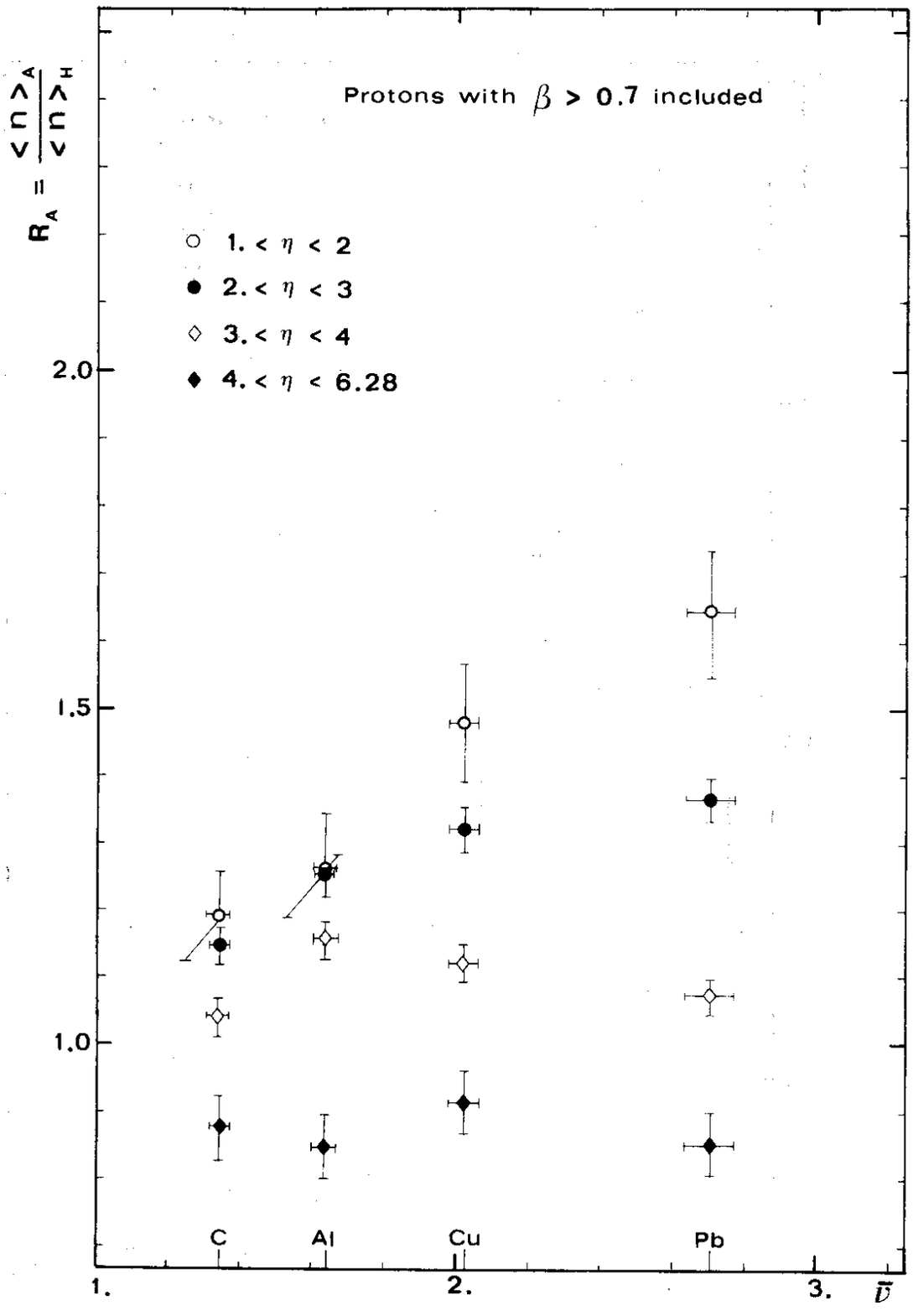
Protons with β > 0.7 included
$R_A = \frac{\langle n \rangle_A}{\langle n \rangle_H}$
1. < η < 2
2. < η < 3
3. < η < 4
4. < η < 6.28
2.0
1.5
1.0
C
Al
Cu
Pb
1.
2.
3.
$\bar{\nu}$

Fig. 3

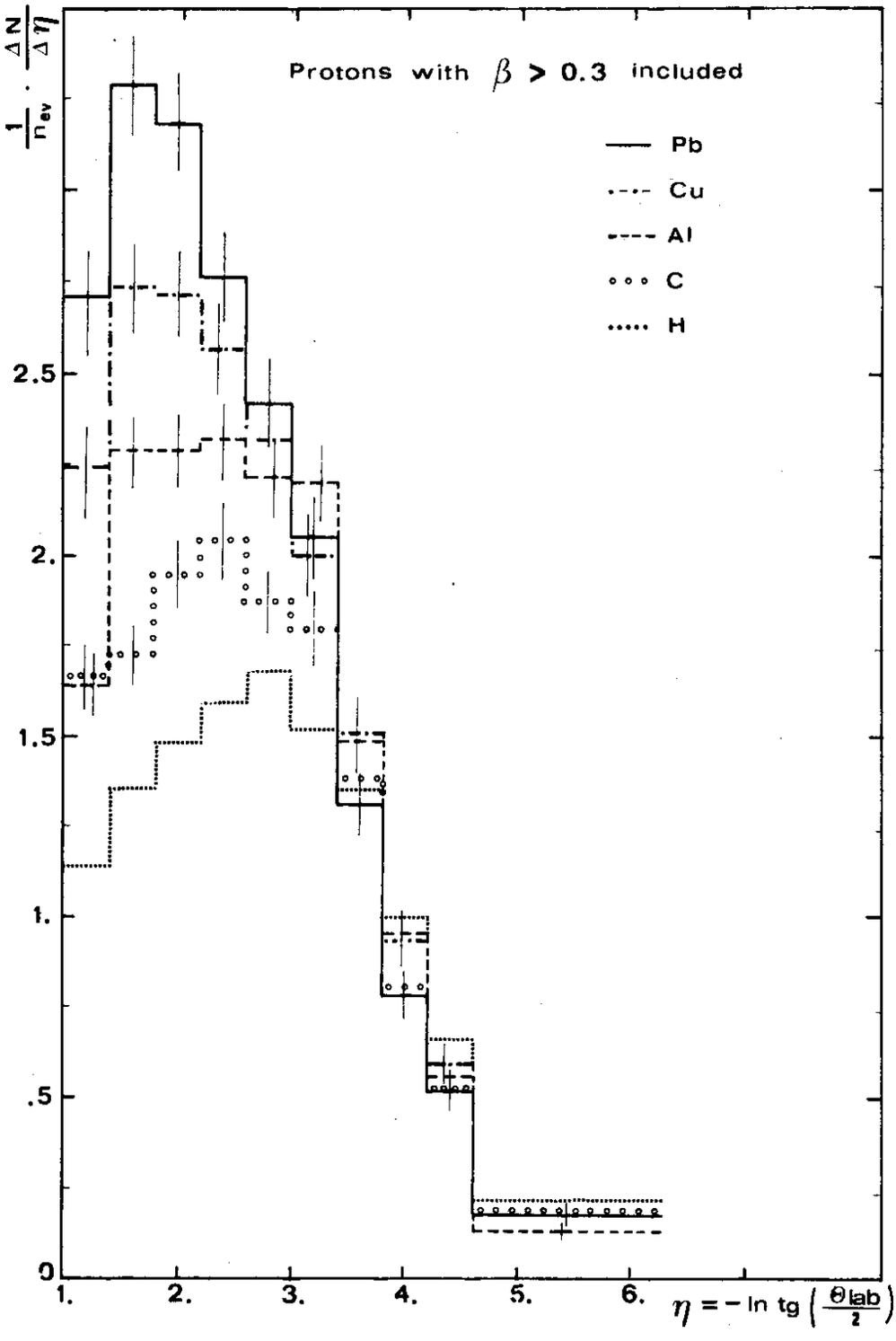
Protons with $\beta > 0.3$ included
Pb
Cu
Al
C
H
$\frac{1}{n_{ev}} \cdot \frac{\Delta N}{\Delta \eta}$
2.5
2.
1.5
1.
.5
0
1.
2.
3.
4.
5.
6.
$\eta = -\ln \mathrm{tg}\left(\frac{\theta_{lab}}{2}\right)$

Fig. 4

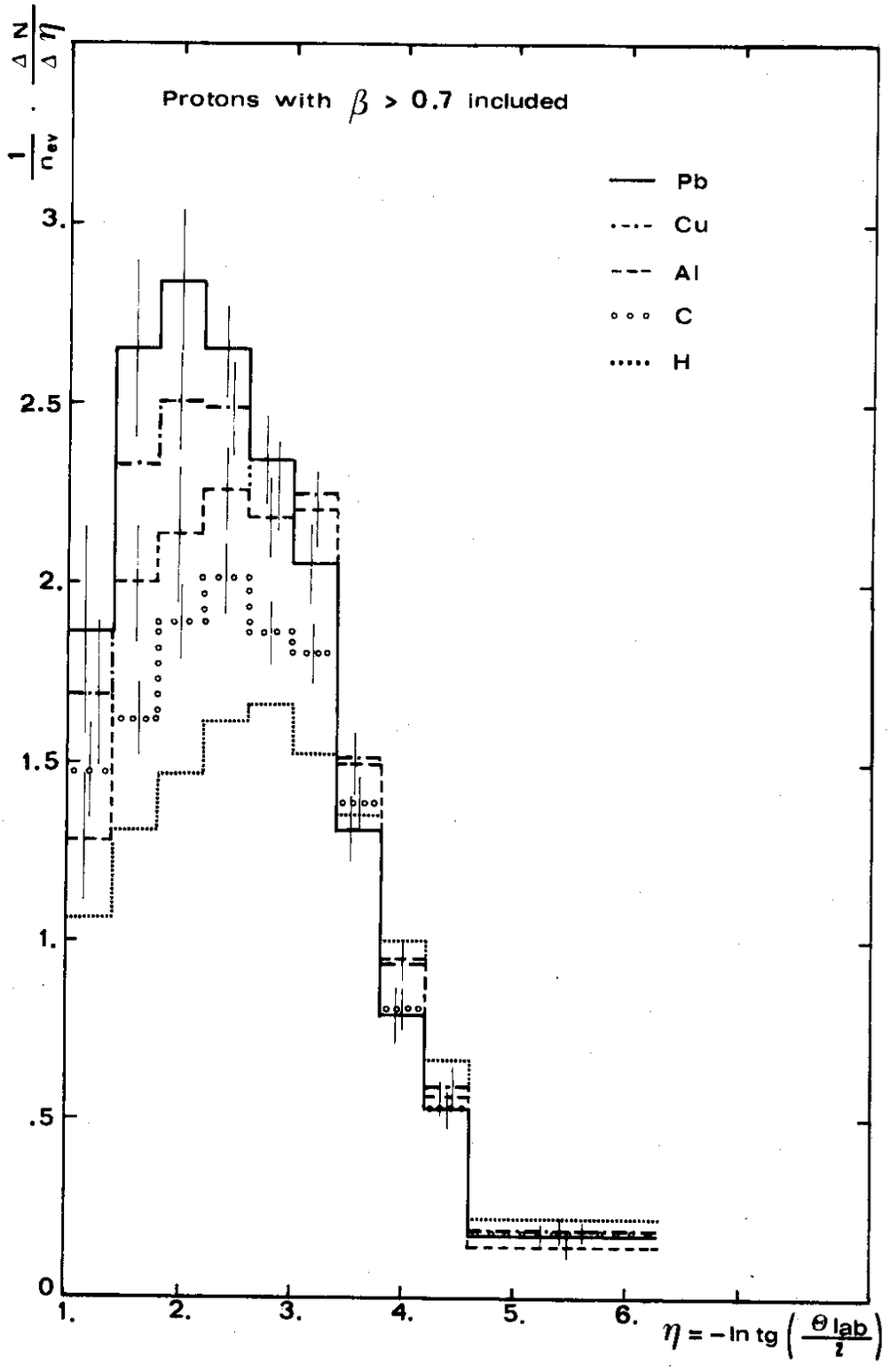
Protons with β > 0.7 included
Pb
Cu
Al
C
H
$\frac{1}{n_{ev}} \cdot \frac{\Delta N}{\Delta \eta}$
3.
2.5
2.
1.5
1.
.5
0
1.
2.
3.
4.
5.
6.
$\eta = -\ln \mathrm{tg}\left(\frac{\theta_{lab}}{2}\right)$

Fig. 5

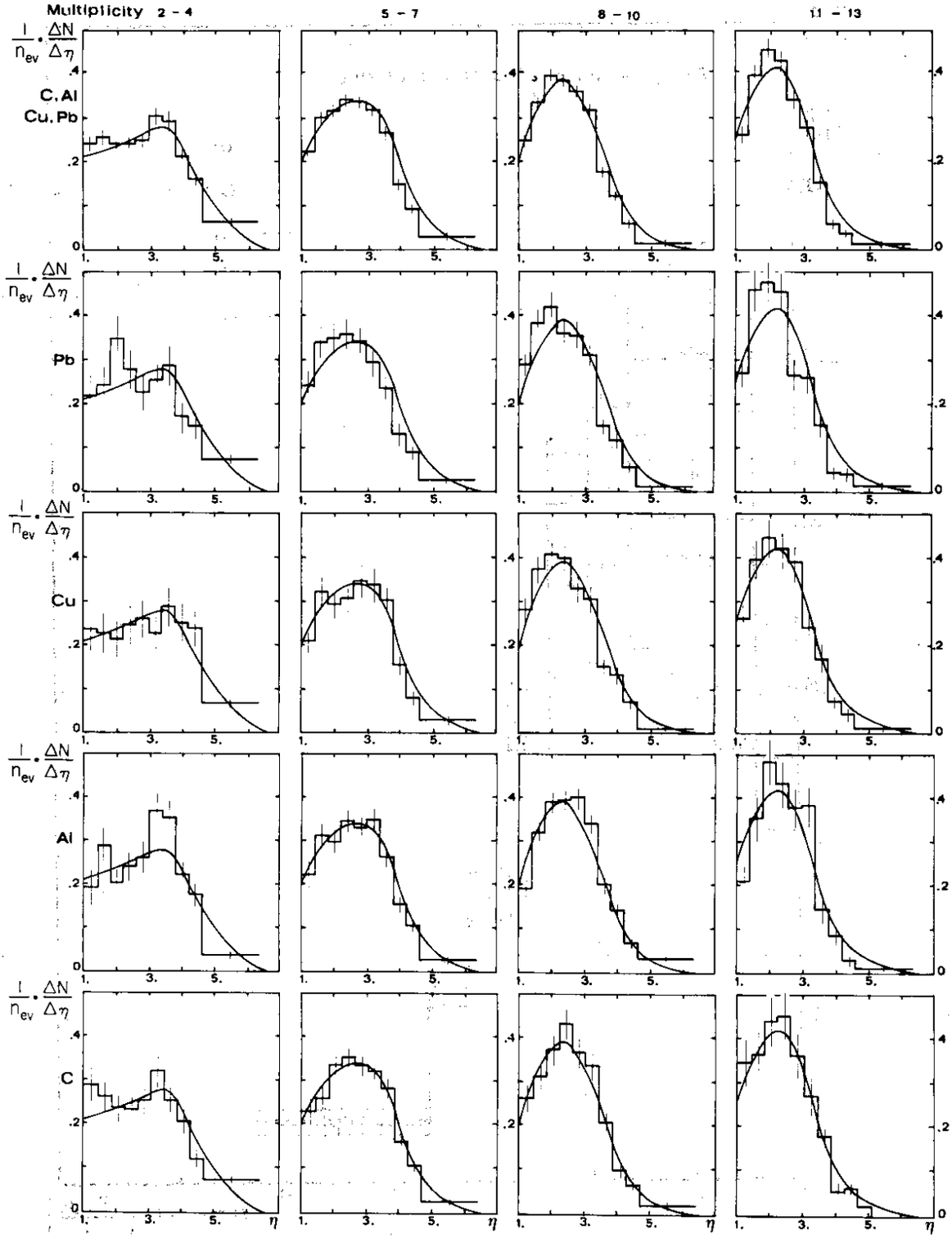
Multiplicity 2 - 4
5 - 7
8 - 10
11 - 13
$\frac{1}{n_{ev}} \cdot \frac{\Delta N}{\Delta \eta}$
C, Al
Cu, Pb
Pb
Cu
Al
C
η

Fig. 6

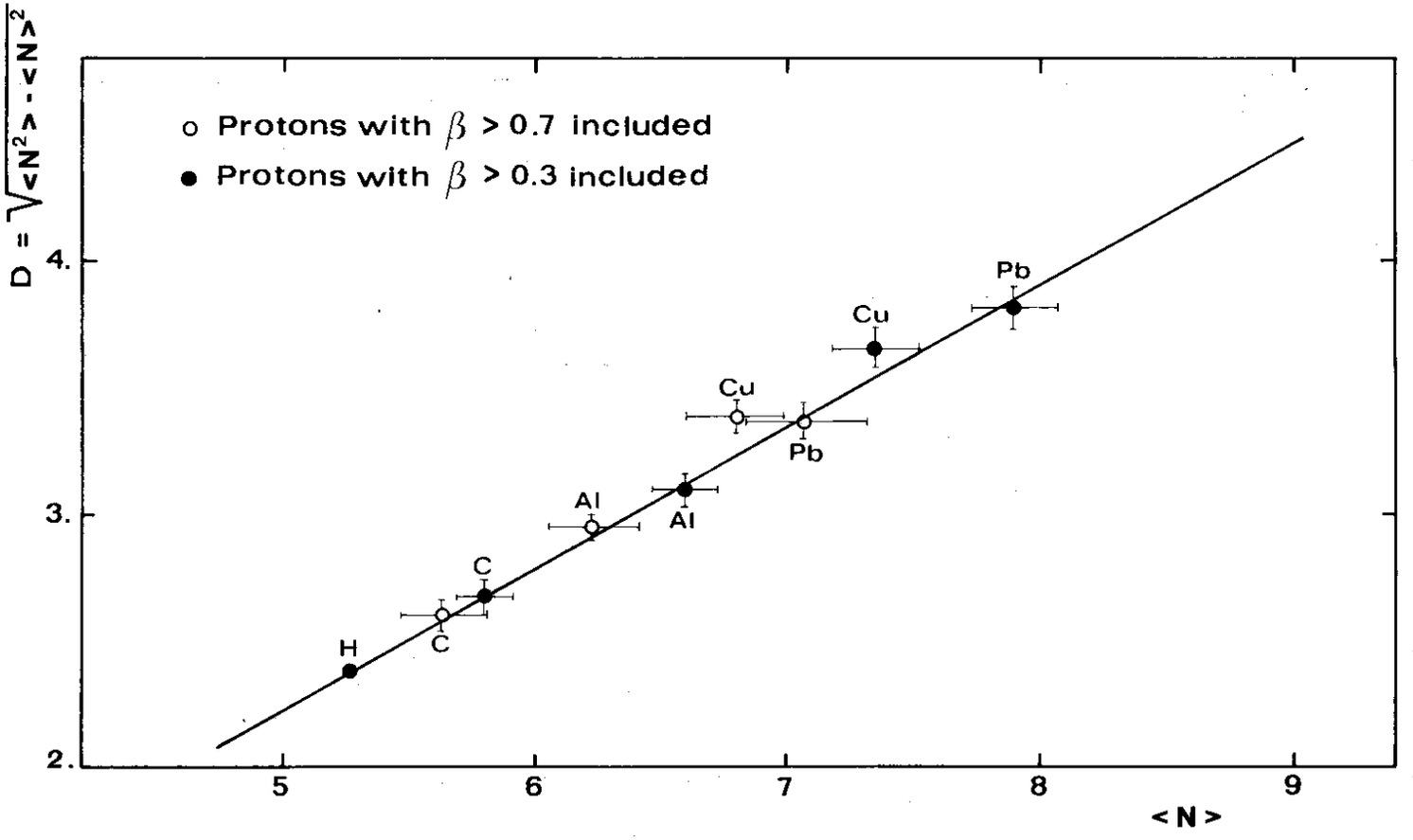
o Protons with β > 0.7 included
● Protons with β > 0.3 included
D = √<N²> - <N>²
4.
3.
2.
5
6
7
8
9
<N>
H
C
C
Al
Al
Cu
Pb
Cu
Pb

Fig. 7

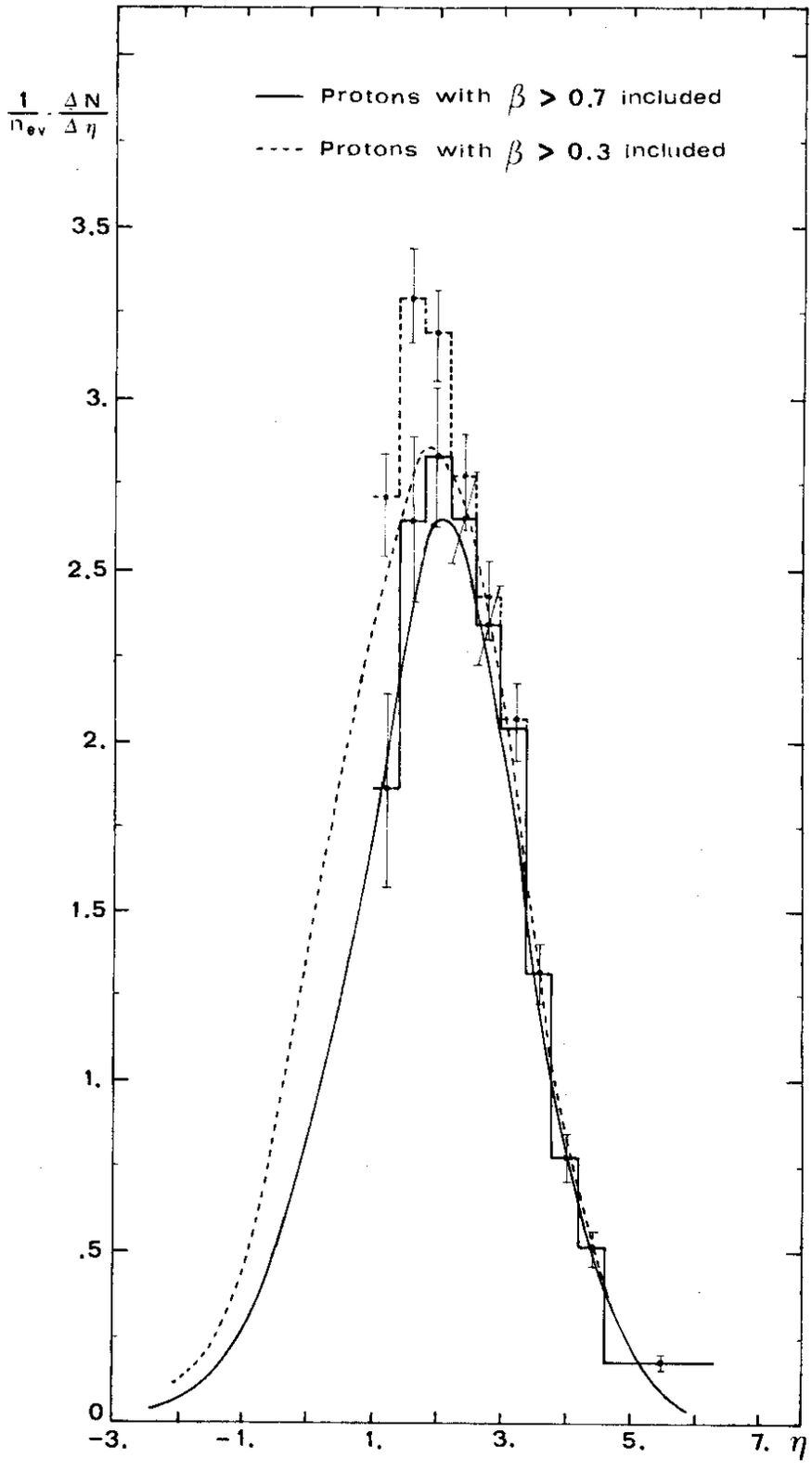
Protons with $\beta > 0.7$ included
Protons with $\beta > 0.3$ included
$\frac{1}{n_{ev}} \cdot \frac{\Delta N}{\Delta \eta}$
3.5
3.
2.5
2.
1.5
1.
.5
0
-3.
-1.
1.
3.
5.
7.
η

Fig. 8

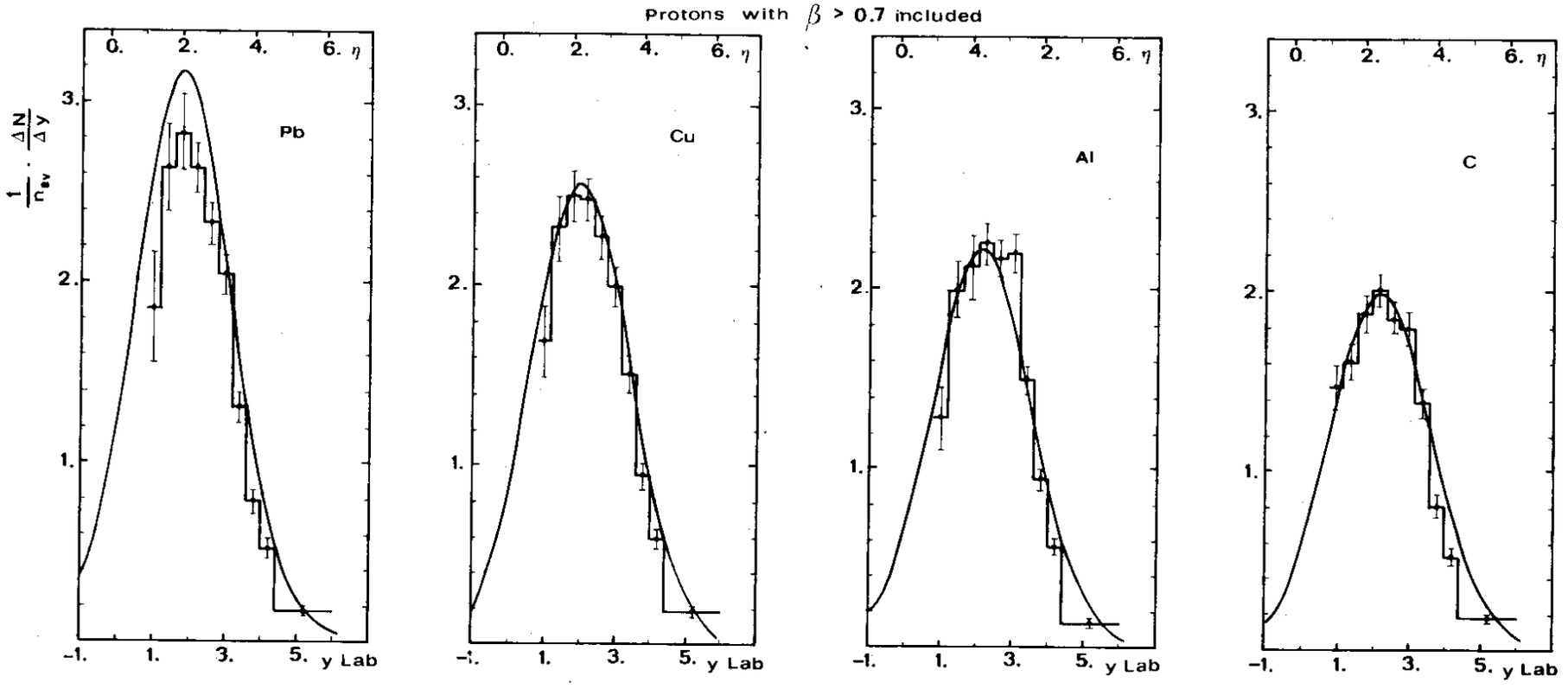
Protons with β > 0.7 included
1/n_ev · ΔN/Δy
Pb
Cu
Al
C
0. 2. 4. 6. η
3.
2.
1.
-1. 1. 3. 5. y Lab

Fig. 9